Food & Function

Grape pomace extract attenuates high fat diet-induced endotoxemia and liver steatosis in mice.

Journal:	*Food & Function*
Manuscript ID	FO-ART-12-2024-006332.R1
Article Type:	Paper
Date Submitted by the Author:	13-Feb-2025
Complete List of Authors:	Muscia Saez, María Victoria; Facultad de Ciencias Médicas, Universidad Nacional de Cuyo, Fisiopatología; Instituto de Medicina y Biología Experimental de Cuyo (IMBECU), Laboratorio de Nutrición y Fisiopatología de la Obesidad Perdicaro, Diahann; Universidad Nacional de Cuyo Facultad de Ciencias Medicas, Fisiopatología; CONICET Mendoza, Laboratorio de Nutrición y Fisiopatología de la Obesidad, Instituto de Medicina y Biología Experimental de Cuyo (IMBECU) Cremonini, E.; University of California Davis, Costantino, Valeria; Consejo Nacional de Investigaciones Cientificas y Tecnicas, Instituto de Medicina y Biología Experimental de Cuyo (IMBECU); Universidad Nacional de Cuyo Facultad de Ciencias Medicas, Ârea de fisiología Patológica Fontana, Ariel R.; IBAM, Facultad de Ciencias Agrarias, Universidad Nacional de Cuyo Oteiza, Patricia; UC Davis, Departments of Nutrition and Environmental Toxicology Vazquez Prieto, Marcela; Universidad Nacional de Cuyo Facultad de Ciencias Medicas, Fisiopatología; CONICET Mendoza, Laboratorio de Nutrición y Fisiopatología de la Obesidad, Instituto de Medicina y Biología Experimental de Cuyo (IMBECU)

Grape pomace extract attenuates high fat diet-induced endotoxemia and liver steatosis in mice

Muscia Saez V.[a1], Perdicaro D. J.[a1], Cremonini E.[b], Costantino V. V. [c], Fontana A. R.[d], Oteiza P. I.[b], Vazquez Prieto M. A.[a*].

[a] Laboratorio de Nutrición y Fisiopatología de la Obesidad, Facultad de Ciencias Médicas, Universidad Nacional de Cuyo e Instituto de Medicina y Biología Experimental de Cuyo (IMBECU)-CONICET, Argentina.

[b] Departments of Nutrition and Environmental Toxicology, University of California, Davis, USA.

[c] Laboratorio de Fisiopatología Renal, Facultad de Ciencias Médicas, Universidad Nacional de Cuyo e Instituto de Medicina y Biología Experimental de Cuyo (IMBECU)-CONICET, Argentina.

[d] Laboratorio de Bioquímica Vegetal, Instituto de Biología Agrícola de Mendoza (IBAM), Facultad de Ciencias Agrarias, CONICET-Universidad Nacional de Cuyo, M5528AHB, Chacras de Coria, Argentina.

1. Equally contributed to this work

*Corresponding author at: Marcela A. Vazquez Prieto, School of Medicine, National University of Cuyo and IMBECU-CONICET, M5502JMA Mendoza, Argentina, Phone: ++54 261 4135000 ext. 2686 / Fax: ++54 261 4494047. mvazquez@fcm.uncu.edu.ar

Abstract

Obesity is a prominent global health concern associated with chronic inflammation and metabolic disorders, such as insulin resistance, type 2 diabetes, and non-alcoholic fatty liver disease (NAFLD). Excessive consumption of saturated fats exacerbates these conditions by increasing intestinal barrier permeability and circulating endotoxins. This study aims to investigate, in a murine model of high-fat diet (HFD)-induced obesity, the potential beneficial effects of a grape pomace extract (GPE), rich in phenolic compounds, at mitigating endotoxemia, and liver steatosis. Underlying mechanisms were characterized in an *in vitro* model of intestinal inflammation and permeabilization, as induced by tumor necrosis factor alpha (TNFα) in Caco-2 cell monolayers. Consumption of a HFD (60% calories from fat) for 13 weeks induced obesity, insulin resistance, and liver damage, evidenced by higher levels of plasma alanine aminotransferase (ALT), hepatic triglycerides content, and steatosis. In addition, HFD caused metabolic endotoxemia, hepatic toll-like receptor 4 (TLR4) upregulation and inflammation. GPE supplementation significantly reduced body weight and subcutaneous and visceral adipose tissue weight, and attenuated metabolic dysregulation. Furthermore, GPE decreased circulating LPS levels and mitigated HFD-mediated hepatic TLR4 upregulation, nuclear factor kappa B (NF-κB) activation, and downstream expression of proteins involved in oxidative stress and inflammation (NOX4, TNFα, and F4/80). In Caco-2 cells, GPE mitigated TNFα-induced monolayer permeabilization, decreased tight junction (TJ) protein levels, enhanced cellular oxidant production, activated redox-sensitive signaling, i.e., NF-κB and ERK1/2, and increased NOX1 and MLCK mRNA levels, being the latter a key regulator of monolayer permeability. The above findings suggest that GPE may protect against HFD-induced obesity and associated metabolic dysfunction (insulin resistance and NAFLD) by modulating intestinal barrier integrity and related endotoxemia.

Abbreviations: **4-HNE**, 4-hydroxynonenal; **ALT**, alanine aminotransferase; **AU**, arbitrary units; **AUC**, area under the curve; **BW,** body weight; **C**, control; **DHE**, dihydroethidium; **GP**, grape pomace, **GPE**, grape pomace extract; **GTT**; glucose tolerance tests; **HFD**, high-fat diet; **HOMA-IR**, homeostasis model assessment parameter; **IFN-γ**, human interferon-gamma; **LMW-PPs**, low molecular weight polyphenols; **LPS**, lipopolysaccharide; **MLCK,** myosin light-chain kinase; **NAFLD**, non-alcoholic fatty liver disease; **NAS**, NAFLD activity score; **NF-κB**, nuclear factor kappa B; **TEER**, transepithelial electrical resistance; **TJ**, tight junction; **TLR4**, toll-like receptor 4; **TNF**α, tumor necrosis factor alpha; **ZO-1**, zonula occludens protein 1.

Keywords: obesity, grape pomace extract, high-fat diet, endotoxemia, hepatic steatosis, intestinal barrier permeability.

1. Introduction

The prevalence of obesity worldwide has increased dramatically in recent decades, constituting one of the most significant public health challenges globally (1). Obesity is a multifactorial disease resulting in excessive accumulation of adipose tissue, being characterized by chronic low-grade inflammation, which contributes to the development of cardiometabolic disorders, such as type 2 diabetes, coronary heart disease (CHD), and nonalcoholic fatty liver disease (NAFLD), among others (2). Changes in eating habits, particularly those associated with high consumption of saturated fats, are linked to low-grade chronic inflammation. This is partly attributed to elevated circulating bacterial lipopolysaccharides (LPS) concentration, a condition called metabolic endotoxemia (3). LPS are outer membrane glycolipids of gram-negative bacteria that, once they reach the circulation, can contribute to the pathogenesis of NAFLD and insulin resistance (4). The integrity of the mucosal barrier plays a crucial role in maintaining intestinal homeostasis and preventing the translocation of harmful substances, such as LPS, from the gut lumen into the circulation. Increased permeability, often referred to as

"leaky gut", allows LPS and other microbial products to enter the bloodstream exacerbating systemic inflammation (5), commonly associated with various pathological conditions, including obesity-related diseases (6). Tight junction (TJ) proteins, such as occludin, claudin-1, and ZO-1, are crucial for maintaining intestinal barrier integrity. Disruption of these proteins, often due to inflammation or gut dysbiosis, increases intestinal permeability (7–9).

In the last decades, NAFLD has become one of the most common chronic liver diseases worldwide, paralleling the increased prevalence of obesity. NAFLD covers a spectrum of liver conditions, from simple steatosis (fat accumulation) to non-alcoholic steatohepatitis (NASH), which can progress to fibrosis, cirrhosis, and even hepatocellular carcinoma (10). In the context of NAFLD, the liver's response to endotoxemia is particularly critical. The activation of the hepatic toll-like receptor 4 (TLR4) signaling pathway by LPS triggers a proinflammatory response through the upregulation of several transcription factors, including Nuclear Factor-kB (NF-kB), a key signaling pathway in driving hepatic inflammation and the progression of liver disease (11).

Dietary bioactive compounds can play an important role in protecting from the harmful effects of Western-style diets. Previous results showed that supplementation with an extract rich in cyanidin and delphinidin protects mice from HFD-induced endotoxemia and liver inflammation (12–15). In addition, the flavan-3-ol epicatechin protects the intestinal barrier from HFD-induced permeabilization, liver steatosis, and insulin resistance (16). Importantly, these flavonoids, abundant in grape pomace (GP), have shown protective effects against various inflammatory and metabolic conditions (17,18). GP, a by-product of wine production, contains high amounts of phenolic compounds, which exhibit antioxidant, anti-inflammatory, and antimicrobial properties (19). A grape seed proanthocyanidin extract attenuated HFD-induced inflammation and adiposity by modulating the gut microbiota in mice (20). We previously observed that supplementation with a GP extract (GPE) attenuated high-fat/high-fructose-induced adiposity, impaired

insulin signaling, liver damage, and inflammation in rats (21). GPE is particularly rich in anthocyanins, with malvidin being the most abundant. Additionally, it contains significant amounts of stilbenes like polydatin, flavanols such as catechins and epicatechins, and hydroxybenzoic acids like gallic and syringic acids. Previous studies from our group have characterized the main GPE metabolites present in plasma and tissues of rats, providing insights into its bioavailability and potential health benefits (22). Recent reviews have highlighted the therapeutic potential of GPE, emphasizing that their rich polyphenol content may underlie their ability to mitigate oxidative stress and inflammation (23).

Based on the above, this study aims to evaluate if supplementing mice with a GPE could mitigate HFD-induced intestinal permeabilization and endotoxemia and how this could be related to the prevention of liver inflammation and steatosis. The underlying mechanisms were characterized in an *in vitro* model of a human intestinal monolayer (Caco-2 cells).

2. Materials and Methods

2.1. Materials

Cholesterol, LDL cholesterol, triglycerides concentrations, and alanine transaminase (ALT) were determined using kits purchased from Wiener Lab. (Rosario, Santa Fe, Argentina). Glucose levels were measured using a glucometer obtained from Accu-Chek Performa, Roche (Bs. As., Argentina). Insulin concentrations were determined using the kit purchased from Crystal Chem (#90060) (Downers Grove, IL, USA). Endotoxin levels were determined using a kit from Abbexa (Cambridge, UK). Antibodies for phospho (Ser176/180) IKKα/β (#2697), IKKα (#2682), p65 (#8242), phospho (Thr202/Tyr204) ERK (#4370), ERK (#9102) and HSC-70 (sc-7298) were obtained from Cell Signaling Technology (Danvers, MA.). TLR4 (sc-293072), TNFα (sc-130349), and F4/80 (sc-377009) were from Santa Cruz Biotechnology *(*Santa Cruz, CA). Antibodies for 4-hydroxynonenal (4-HNE) (ab46545), NOX4 (ab129068) and phospho (S536) p65

antibody (ab7630) were purchased from Abcam, Inc. (Cambridge, MA). Antibody for β-actin (A1978) was from Sigma-Aldrich, St. Louis, MO, USA. Antibodies for ZO-1 (33-9100), occludin (33-1500), and claudin-1 (71-7800) were from Invitrogen (Carlsbad, CA). Hematoxylin and eosin solutions were obtained from Biopack (Buenos Aires, Argentina). Nitrocellulose membranes were obtained from Bio-Rad (Hercules, CA). HBSS 1X (21-022-CV) was obtained from Corning (Manassas, VA). Human interferon-gamma (IFN-γ) was obtained from Cell Signaling Technology (Danvers, MA). Dihydroethidium (DHE) was from Sigma Chem. Co. (St. Louis, MO).

2.2. Phenolic compounds characterization of grape pomace extract (*GPE)*

The GPE was provided by the Institute of Agricultural Biology of Mendoza (IBAM), Faculty of Agrarian Sciences, CONICET-National University of Cuyo (Argentina). GPE was obtained from Vitis vinifera L. cv. Malbec located in Gualtallary, Mendoza, Argentina. The phenolic compounds from the GPE were obtained by solid-liquid extraction according to the method described by Antoniolli et al. (24). Five mg of the lyophilized GPE were dissolved in 1 mL of the initial mobile phase corresponding to the method for non-anthocyanin compounds reported by Ferreyra et al. and submitted to phenolic characterization by LC-DAD-FLD. Anthocyanins were quantified according to the method reported by Fontana et al.(25).

The total phenolic content (TPC) was determined by the FolinCiocalteu assay according to Antoniolli et al. (26). TPC was expressed as milligrams of gallic acid equivalents (GAE) per gram of sample by using a calibration curve with GAE (three replicates) in a range between 0–200 mg L−1 (R2 = 0,9963). Absorbance measurements were made with a UV–vis spectrophotometer (Cary-50, Varian Inc., Walnut Creek, CA).

2.3 Animals and Animal Care

All animal procedures were approved by the Institutional Animal Care and Use Committee of the School of Medical Science, National University of Cuyo (Protocol approval Nº 240/2023).

Healthy male C57BL/6 mice (20–25 g) (8-9 mice/group) were fed for 13 weeks either: A- a diet containing approximately 10% total calories from fat (C) (TD.08806, Harlan Laboratories, Madison, WI), B- a diet containing approximately 60% total calories from fat (lard) (HF) (TD.06414, Harlan Laboratories, Madison, WI), C- the control diet supplemented with 300 mg GPE/kg body weight (BW)/day (C+GPE), and D- the HFD supplemented with 300 mg GPE/kg BW/day (HF+GPE). Mice consumed the GPE daily as part of their diet, ensuring a consistent intake throughout the study. Both the C and HF diets were ground to a fine powder and then re-pelleted after the addition of the corresponding amount of GPE, which was added as a lyophilized ground powder. GPE-containing diets were prepared every week to account for changes in body weight and food intake and were kept at −20°C until use to prevent potential phenolic compound degradation as previously described (26). The dose of GPE was selected based on our earlier research (21,25,26) and considering that it delivers a physiological level of phenolic compounds achievable through regular dietary intake, corresponding to a human equivalent dose of 305 mg per day of total phenolic compound.

BW and food intake were measured weekly throughout the study, as previously described (26). After 13 weeks of the dietary treatments, and following an 8-hour fast, mice were anesthetized with Ketamine (80 mg/kg BW) and Diazepam (10 mg/kg BW), and were euthanized by intracardiac puncture, following institutional and ethical guidelines. Blood was collected from the abdominal aorta into heparinized tubes, and plasma was isolated after centrifugation at 3000 x g for 10 min at room temperature. Liver and adipose tissue were collected, and flash-frozen in liquid nitrogen and then stored at −80°C for further analysis. Visceral adipose tissue (vWAT) was defined as the

sum of mesenteric, epididymal, and retroperitoneal fat depots, while subcutaneous adipose tissue (sWAT) included dorsolumbar, inguinal, and gluteal fat depots.

2.4. Metabolic measurements

Blood glucose levels were assessed using a glucometer on samples collected from the tail vein. Briefly, glucose tolerance tests (GTT) were performed after 10 weeks on the respective diets as previously described (18). For GTT, mice were fasted for 8 hours and subsequently administered D-glucose (2 g/kg body weight) via injection. Blood glucose was measured at 0 (baseline) and at 30, 60, 90, and 120 minutes post-injection, following established protocols (21,27,28). After the study concluded, plasma concentrations of total cholesterol, LDL cholesterol, triglycerides and alanine transaminase (ALT) were quantified using enzymatic colorimetric assays with commercially available kits. Endotoxin levels were quantified in plasma with an Endotoxin ELISA Kit. Insulin levels were measured with an Ultra-Sensitive Insulin ELISA kit, and insulin resistance was evaluated by calculating the homeostasis model assessment of insulin resistance (HOMA-IR) using the formula: HOMA-IR (mg/dl × μU/ml) = fasting glucose (mg/dl) × fasting insulin (μU/ml)/22.5.

2.5. Determination of liver triglycerides content

Liver triglyceride content was analyzed after extraction and saponification, following the procedure described by Weber et al., with minor modifications (15,27). Briefly, a 100 µl aliquot of 10% (w/v) liver homogenate was mixed with 300 µl of a KOH (30% w/v) ethanol (1:2, v/v) solution and evaporated overnight at 55°C. The next day, 1 ml of 50% (v/v) ethanol was added, and the samples were centrifuged for 5 minutes at 10,000 x g at room temperature. From the resulting supernatant, 200 µl were taken and mixed with 215 µl of 1 M $MgCl_2$ and placed on ice for 10 minutes. After centrifugation at 10,000 x g for 5 minutes at room temperature, 10 µl of the supernatant was assayed for triglyceride content using the Wiener Lab enzymatic triglyceride determination kit.

2.6. Histological analysis of liver tissue

Formalin-fixed liver tissue was processed, and 5-μm-thick paraffin sections were stained with hematoxylin and eosin (H&E) and examined using a Nikon 80i microscope (Nikon, Japan) as described by Cremonini et. al. (12). Hepatic histological examination was conducted according to the histological scoring system to assess the NAFLD activity score (NAS) proposed by Kleiner et al. (29). Three randomly selected fields per animal were evaluated by a pathologist, who was blinded to the group identities. All liver specimens were analyzed using ImageJ software (version 1.53t, National Institutes of Health, Bethesda, MD).

2.7. Caco-2 cell culture and assessment of monolayer permeability

Caco-2 cells were procured from the American Type Culture Collection (ATCC) (Rockville, MA). Cell culture media and reagents were sourced from Invitrogen/Life Technologies (Grand Island, NY). Caco-2 cells were cultured at 37°C in a 5% (v/v) CO_2 atmosphere in Minimum Essential Medium (MEM) supplemented with 10% (v/v) fetal bovine serum, antibiotics (50 U/mL penicillin, and 50 μg/mL streptomycin), 1% (v/v) of 100X non-essential amino acids, and 1 mM sodium pyruvate. The medium was replaced every 3 days during cell growth and differentiation. For the experiments, cells cultured in 6-well plates were used 12 days after reaching confluence, while cells grown on inserts were used 21 days after confluence to allow for differentiation into intestinal epithelial cells. Cells were used between passages 3 and 15. All experiments were performed in serum- and phenol-red-free MEM.

Monolayer permeability was assessed by measuring the transepithelial electrical resistance (TEER) as previously described (12). Briefly, cells were grown for 21 days on transwell inserts (12 mm, 0.4 μm pore polyester membranes) in 12-well plates (0.3×10^6 cells/transwell). For the experiments, Caco-2 cell monolayers were preincubated for 24 h with IFN-γ (10 ng/ml) added to the basolateral compartment to upregulate the TNFα

receptor. Monolayers were then pre-incubated for 30 min in the presence or absence of 25 µg/ml GPE added to the upper compartment. Subsequently, cells were treated with or without TNFα (10 ng/ml) added to the lower compartment for 6 hours. For TEER assessment, incubation media were removed from the upper and lower compartments, cells were rinsed with HBSS 1X, and the same solution was added to both compartments to perform the measurement. The monolayers were used when TEER values were between 350–450 Ω cm^2. TEER was measured using a Millicell-ERS Resistance System (Millipore, Bedford, MA) and calculated as TEER = (Rm – Ri) × A (where Rm is the transmembrane resistance; Ri is the intrinsic resistance of a cell-free media, and A is the surface area of the membrane in cm^2). Arbitrary units (AU) were calculated based on TEER values for the non-treated (control) cells.

2.8. Cell viability

Cell viability was assessed using the MTT (3-[4,5-dimethylthiazol-2-yl] -2,5 diphenyl tetrazolium bromide) assay, which measures the conversion of MTT to formazan crystals by viable cells. Cells were grown in 96-well plates for 12 days. Caco-2 cells were pre-treated with IFN-γ (10 ng/ml) for 24 h. Subsequently, the medium was removed and cells were treated with or without TNFα (10 ng/ml) in the presence or absence of GPE 25 µg/ml for 6 hours. After the incubation period, the medium was removed and cells were incubated with a 0.5 mg/mL MTT solution in PBS for 1 hour at 37°C. Then the reaction was stopped by the addition of 0.01 N HCl containing 10% (w/v) SDS, and plates were then incubated overnight. Differences in absorbance (λ570-λ690 nm) was determined using a BioTek Synergy H1 plate reader (BioTek Instruments, Winooski, VT) and normalized by values for the control (non-added) cells (30).

2.9. Cell oxidant levels

Cell oxidant levels were assessed using dihydroethidium (DHE). DHE penetrates cells and, upon oxidation, is transformed into fluorescent compounds. Caco-2 cells were

cultured and differentiated in 96-well plates for 12 days and then were pre-treated with IFN-γ (10 ng/ml) for 24 h. After removing the medium, the cells were pre-incubated for 30 minutes in the absence or presence of 25 μg/ml GPE and then the cells were treated with or without TNFα (10 ng/ml) for 10 minutes. The medium was removed and cells were incubated with 25 μM DHE (in serum- and phenol red-free MEM) for 30 min at 37°C in the dark. After incubation, the DHE was removed, cells were rinsed with PBS, and fluorescence was measured for oxidized DHE at λexc 485 nm and λem 535 nm. To account for differences in cell number, DHE fluorescence was normalized to protein content using the sulforhodamine B (SRB) assay as described in Iglesias et al. (30).

2.10. RNA isolation and Quantitative PCR (qPCR)

For qPCR studies, RNA was extracted from cells using TRIzol reagent (Invitrogen) following the manufacturers' instructions. The cDNA was generated using high-capacity cDNA Reverse Transcriptase (Applied Biosystems). mRNA levels of NOX1, MLCK, and β-actin were assessed by qPCR (iCycler, Bio-Rad, Hercules, CA) using the following primers:

Primer NOX1 *Forward*: 5′-GTACAAATTCCAGTGTGCAGACCAC-3′

Primer NOX1 *Reverse*: 5′-GTACAAATTCCAGTGTGCAGACCAC-3′

Primer MLCK *Forward*: 5′-GAGGTGCTTCAGAATGAGGACG -3′

Primer MLCK *Reverse*: 5′- GCATCAGTGACACCTGGCAACT -3′

Primer β-Actin *Forward*: 5′-TCATGAAGTGTGACGTGGACATCCGC-3′

Primer β-Actin *Reverse: 5′-CCTAGAAGCATTTGCGGTGCACGATG-3′*

The Ct values were normalized to β-actin used as a housekeeping gene. Gene expression was determined using the $2^{-\Delta\Delta Ct}$ method (31).

2.11. Western blot analysis

Tissue and cell total homogenates were prepared as previously outlined (17). Protein concentration was determined using the Bradford method (32). Aliquots of total homogenates containing 30-50µg of protein were denatured with Laemmli buffer, separated by reducing 8–15% polyacrylamide gel electrophoresis, and transferred to PVDF membranes. Colored (Bio-Rad Laboratories, Hercules, CA) and biotinylated (Cell Signaling Technologies, Danvers MA) molecular weight standards were run simultaneously. Membranes were then blocked for 5 minutes with EveryBlot Blocking Buffer from BioRad (Hercules, CA, USA) and subsequently incubated overnight at 4°C with the respective primary antibodies (at a dilution of 1:750 or 1:1000 v/v) in EveryBlot Blocking buffer. After a 90-minute incubation at room temperature with the secondary antibodies (either HRP-conjugated or biotinylated, followed by 1-hour incubation with streptavidin) (at a dilution of 1:10000 v/v), the conjugates were visualized using enhanced chemiluminescence. Images were captured using a Luminescent Analyzer Image Reader (LAS-4000) (Fujifilm, Japan) and the Bio-Rad ChemiDoc Imager, and bands were quantified using the NIH Image J software and ImageLab software (Bio-Rad, Hercules, CA).

2.13. Statistical analysis

Statistical analysis was performed using GraphPad Prism 8.0.1 (GraphPad Software, San Diego, CA, USA). All values are shown as means ± standard error of the means (SEM). Data were analyzed by one-way or two-way analysis of variance (ANOVA) followed by Tukey's Multiple Comparison Test for post-hoc analysis. Changes in body weight were analyzed using repeated measures ANOVA with Tukey's Multiple comparison test. A P value <0.05 was considered statistically significant.

3. Results

3.1. Chemical characterization of GPE.

The content of low molecular weight polyphenols (LMW-PPs) and individual anthocyanins in Malbec GPE are shown in Tables 1 and 2, respectively. The most abundant flavonoids in the extracts were the flavan-3-ols (+)-catechin and (-)-epicatechin, along with the stilbene polydatin (**Table 1**). **Table 2** summarizes the individual anthocyanin concentrations in GPE, categorized by derivative type (nonacylated, acylated, and coumarylated). Regarding concentration, malvidin-3-*O*-glucoside was the predominant anthocyanin, followed by malvidin-3-p-coumaroyl glucoside and petunidin-3-*O*-glucoside.

3.2. GPE supplementation attenuates HFD-induced obesity and insulin resistance.

To examine the effects of GPE on obesity-associated metabolic alterations, male C57BL/6 mice were fed control or HFD diets, with or without GPE supplementation. The average daily food intake was similar across all groups, regardless of the type of diet, although caloric intake was higher in the HF groups compared to the C groups. (**Table 3**)**.** Chronic consumption of HFD caused an increase in BW compared to the C group starting from week 5, and compared to the C+GPE group starting from week 7. GPE supplementation to HFD-fed mice had significantly lower body weight gain than HF mice starting at week 11 (**Figure 1A**). Thus, at the end of the experimental protocol, mice in the HF group had higher BW than mice fed the control diet (44% and 47% higher than the C and C+GPE, respectively). GPE supplementation to HFD-fed mice resulted in a significantly lower BW (17%) at week 13 compared to the HF group (**Table 3**). In accordance with the BW increase observed in the HF group, the weight of both visceral and subcutaneous adipose tissue was also significantly higher compared to the control groups (C and C+GPE) and the HF+GPE group. Specifically, the weight of visceral adipose tissue was 153% and 96% higher in the HF group compared to the C and C+GPE groups, respectively, and 28% lower in the HF+GPE group compared to the HF group. Similarly, the weight of subcutaneous adipose tissue was 171% and 107% higher in the HF group compared to the C and C+GPE groups, respectively, and 31% lower in

the HF+GPE group compared to the HF group. In addition, GPE significantly reduced liver weight compared to the control groups (C and C+GPE) and HF groups.

Chronic HFD feeding induced several metabolic alterations, such as dyslipidemia and insulin resistance, evidenced by elevated fasting blood glucose, insulin levels, and HOMA-IR compared to C and C+GPE groups (**Table 3**). Furthermore, HF mice showed a significantly higher plasma concentration of both total and LDL cholesterol compared to both control groups. GPE supplementation to HFD-fed mice significantly reduced fasting glucose and insulin levels, thereby improving the HOMA-IR and preventing the elevation of plasma triglyceride concentration compared to the HF group. During the intraperitoneal glucose tolerance test (GTT), HFD-treated mice showed a diminished capacity to clear glucose from the circulation compared to both control groups, while GPE supplementation attenuated HFD-induced altered glucose tolerance response (**Figure 1B**). Accordingly, the area under the curve (AUC) for the GTT in HF mice was 128% and 100% higher than in the C and C+GPE groups, respectively. GPE supplementation mitigated the increase in the AUC of GTT caused by the HFD, although the values remained significantly higher than those for the C groups (**Figure 1C**). Together, the above data indicate that GPE consumption mitigated HFD-induced obesity and associated metabolic alterations.

3.3. GPE supplementation attenuated HFD-induced endotoxemia and liver TLR4 activation.

Obesity and consumption of diets rich in saturated fats can cause metabolic endotoxemia and consequently promote inflammation. LPS proinflammatory action is mediated through its interaction with TLR4. Therefore, we next evaluated the plasma LPS concentration and liver TLR4 protein levels by Western blot. As expected, consumption of the HFD caused endotoxemia, being LPS concentration in the HF group significantly higher compared to the C and C+GPE groups (45% and 37%, respectively). GPE supplementation mitigated HFD-induced endotoxemia (28% lower than HF) (**Figure 2A**).

Accordingly, hepatic TLR4 protein levels were significantly higher in the HF group compared to both control groups, while GPE supplementation prevented HFD-induced TLR4 upregulation (**Figure 2B**).

3.4. Effect of GPE on HFD-induced liver steatosis

We next evaluated the effects of the HFD and GPE supplementation on the development of liver damage and steatosis. HFD caused a significant increase in hepatic triglyceride content (35 and 44% compared to the C and C+GPE groups respectively). Furthermore, the activity in plasma of the liver enzyme ALT, measured as a marker of liver injury, was also significantly higher in HF mice compared to C and C+GPE groups (128% y 236% respectively) (**Figure 3A and B**). GPE supplementation to HFD-fed mice prevented both the accumulation of liver triglycerides and elevated levels of ALT, to values comparable to those in the control groups. Representative liver images from the four dietary groups are shown in **Figure 3C**. Histological analysis of H&E-stained liver sections (**Figure 3D**) revealed significantly higher NAFLD Activity Score (NAS) in the HF group compared to the C and C+GPE groups (**Figure 3E**). Mice fed the HFD supplemented with GPE exhibited a 57% lower NAS than the HF group.

3.5. Effects of GPE supplementation on NF-κB activation and downstream expression of proteins involved in inflammation and oxidative stress.

TLR4-ligand binding leads to the activation of the nuclear transcription factor kappa B (NF-κB) and the downstream expression of proteins involved in inflammation and oxidative stress. Consumption of the HFD led to the activation of the NF-κB pathway, as evidenced by higher phosphorylation of IKKα/β (Ser178/180) (45% and 38% compared to de C and C+GPE respectively) and p65 (Ser536) (58% and 63% compared to both control groups). GPE supplementation significantly reduced HF-induced phosphorylation of IKKα/β by 24%, but did not affect p65 phosphorylation (**Figure 4A**).

NADPH oxidase (NOX) is the primary enzymatic source of reactive oxygen species, which can lead to oxidative stress upon chronic activation. Therefore, we next evaluated NOX4 protein levels and, as parameter of oxidative stress, the adducts of proteins 4-hydroxynonenal (4-HNE), a product of lipid oxidation (**Figure 4B**). Additionally, protein levels of the cytokine TNFα and the macrophage marker (F4/80) were evaluated in the liver by western blot (**Figure 4C**). Mice fed the HFD showed a significant upregulation of NOX4, F4/80, and TNFα and increased 4-HNE levels compared to the C groups (29%, 43% and 82% respectively). Except for 4-HNE, GPE supplementation to HFD-fed mice prevented the above alterations (reducing 23%, 31%, and 35% respectively) supporting GPE's protective effects against inflammation and oxidant production in the context of HFD and obesity.

*3.6. GPE prevents TNF*α*-induced Caco-2 monolayer permeabilization and decreased TJ protein levels.*

Increased endotoxemia can be due to greater intestinal permeability. We next evaluated the capacity of GPE to protect TNFα-induced permeabilization of Caco-2 cell monolayers by measuring the transepithelial electrical resistance (TEER). First, a cell viability assay was performed using the MTT assay to assess potential cytotoxic effects of the treatments. No changes in cell viability were observed after pre-incubating cells for 30 minutes with GPE (25 μg/ml) and for a further 6 h in the absence or the presence of TNFα (**Figure 5A**). Incubation for 6 h with TNFα, added to the lower chamber, reduced TEER by 25% compared to the non-added cells (control), which was prevented by GPE (**Figure 5B**). According with an alteration of barrier integrity, TNFα caused a reduction in the protein levels of the TJ proteins occludin (55%), ZO-1 (36%), and claudin-1 (24%) compared to control cells (**Figure 5C**). GPE prevented TNFα-mediated decreased protein levels of occludin and ZO-1, while it did not modify those of claudin-1.

*3.7. Effects of GPE on TNF*α*-mediated activation of pathways that lead to Caco-2 monolayer permeabilization*

TNFα binding to its membrane receptor is associated with NOX activation, which leads to increased production of oxidants, such as superoxide anion and hydrogen peroxide, which, in turn, may contribute to intestinal permeabilization. Therefore, we next measured cellular oxidant production using dihydroethidium (DHE). Caco-2 cells treated with TNFα showed increased DHE oxidation by 30% compared to non-added (control) cells, while pre-treatment with GPE (25 μg/ml) fully prevented this increase (**Figure 6A**). It has been shown that exposure Caco-2 cells to TNFα for a long period of time lead to NOX1 increased expression (14). Accordingly, after 6 h incubation with TNFα we observed a 30% increase in NOX1 mRNA levels, which was prevented by the GPE (**Figure 6B**) Subsequently, we evaluated the mRNA levels of MLCK, the key kinase regulating the opening of the TJ. TNFα treatment significantly increased (2.25-fold) MLCK mRNA levels compared to control values, which was prevented when cells were incubated with the GPE (**Figure 6B**). MLCK expression is in part regulated by NF-κB and ERK1/2, two cell signals activated by increased oxidant production. Thus, we next measured the effects of the GPE on the activation NF-κB (phosphorylation of p65 at Ser536) and ERK1/2 (phosphorylation of ERK1/2 at Thr202/Tyr204) (**Figure 6C**). TNFα caused a significant increase (36 and 74% respectively) in the levels of phosphorylated p65 and ERK1/2 compared to control values. GPE prevented TNFα-mediated increase in p65 phosphorylation, but not that of ERK1/2 (**Figure 6C**).

4. Discussion

This study showed that GPE supplementation attenuates HFD-induced obesity and the main associated metabolic alterations, i.e., insulin resistance, dyslipidemia, hepatic damage, and steatosis. Furthermore, GPE prevented the increased endotoxemia caused by HFD, suggesting that GPE could act at the gastrointestinal tract level mitigating intestinal permeabilization. Supporting these *in vivo* findings, GPE prevented TNF-induced Caco-2 monolayer permeabilization, restoring TJ protein levels and modulating redox-sensitive signals that cause TJ opening.

Obesity, primarily driven by the consumption of diets rich in saturated fats and sugars, represents a global health problem with multiple associated comorbidities (33). Thus, dietary approaches to manage this condition are crucial. We observed that chronic consumption of HFD for 13 weeks significantly increased BW, accompanied by an accumulation of visceral and subcutaneous WAT, hyperglycemia, insulin resistance, and dyslipidemia. Interestingly, even though both HF groups consumed similar amounts of food and calories, supplementation with GPE significantly reduced BW, adipose tissue accumulation, insulin resistance, and attenuated dyslipidemia. Previous evidence, mainly from *in vivo* or *in vitro* studies supports the protective effects of polyphenols or polyphenols-rich food against diet-induced obesity, adiposity, and their associated metabolic consequences mainly related to their anti-inflammatory and redox-regulatory actions (18,34–36). Studies in humans are scarce however, in a cross-over randomized clinical trial in subjects with at least two factors of metabolic syndrome, supplementation during 6 weeks with grape pomace from Tempranillo cultivar (8 g/d) significantly improved fasting insulinemia (37).

Of note, the liver plays a central role in regulating whole-body glucose and lipid metabolism. Excessive dietary fat consumption promotes liver steatosis, which, in turn, can lead to the development and progression of NAFLD (38,39). We observed that GPE supplementation protects the liver from the harmful effects of HFD since plasma levels of ALT, hepatic triglyceride content, and NAS score were comparable to control values. Consistently, phenolic compounds present in GPE, such as epicatechin, quercetin, cyanidin and delphinidin, have demonstrated protective effects against HFD-induced liver damage in rodent models (12,16,36,40).

High fat-induced endotoxemia is also a condition closely linked to the progression of NAFLD and steatohepatitis (39,41–45). Diets rich in fat are associated with a dysfunctional intestinal barrier, which impairs its ability to prevent the translocation of bacterial endotoxins, such as LPS, from the gut into the circulation (42). When this

condition is sustained over time, elevated levels of LPS trigger chronic systemic inflammation, which activates inflammatory pathways that exacerbate liver injury. LPS binding to TLR4 in the liver can lead to the activation of several signaling pathways, including NF-κB and ERK1/2, which stimulate the production of proinflammatory cytokines and cause systemic inflammation and oxidative stress (46–48). In accordance, our results demonstrated that HFD-induced endotoxemia, overexpression of TLR4, accompanied by downstream activation of NF-κB (high IKK and p65 phosphorylation levels) and increased parameters of oxidative stress (NOX4 and 4-HNE-protein adducts) in the liver. NOX enzymes generate superoxide anion and H_2O_2, which contribute to the inflammatory response and subsequent tissue damage (49,50). GPE supplementation prevented the elevated plasma LPS levels observed in HFD-fed mice and protected the liver from inflammation and oxidative stress. Different studies show evidence of the role of grape polyphenols in protecting the gastrointestinal tract and the associated endotoxemia. Grape seed proanthocyanidin extract (500 mg/kg BW) mitigated high-fat/high-carbohydrate diet-induced oxidative stress and protected the intestinal barrier in rats, reducing gut reactive oxygen species levels and endotoxemia-related inflammation mediated by LPS (51). Also, the administration of red and white GP (100 and 500 mg/kg BW, respectively) suppressed chronic inflammation induced by LPS in rats (52). In this study, we did not evaluate the effects of GPE at the gastrointestinal tract. Therefore, further studies are needed to confirm the regulation of the gut-liver axis by GPE.

The intestinal barrier's integrity is maintained by TJ proteins, such as occludin, claudin-1, and ZO-1, that regulate the passage of ions, water and molecules through the paracellular pathway (53,54). The MLCK pathway regulates epithelial barrier function by modulating TJ dynamics proinflammatory stimuli like TNFα disrupt TJ function by activating NF-κB and ERK1/2 pathways and increasing the expression of the MLCK gene leading to increased intestinal permeability (55,56). Consequently, we observed that TNFα reduced TJ protein levels and increased inflammatory and oxidative stress

markers, activating NF-κB and ERK1/2 and leading to TJ opening by MLCK upregulation in Caco-2 monolayer. Most of these adverse events triggered by TNFα were mitigated by the GPE. Accordingly, the flavan-3-ol epicatechin and the anthocyanidins cyanidin and delphinidin, important phenolic compounds found in GPE, inhibit TNFα-mediated monolayer permeabilization, preserve TJ structure and inhibit the disruption of this barrier (15,57). Moreover, a polyphenolic extract obtained from red wine decreased the paracellular permeability in HT-29 colon epithelial cells exposed to proinflammatory cytokines (58). Therefore, our results show that GPE mitigates Caco-2 cell monolayer permeabilization induced by a proinflammatory stimulus by preserving TJ integrity and regulating redox-sensitive mechanisms that modulate TJ opening.

These findings highlight the potential benefits of using winemaking residues, rich in bioactive compounds, as a low-cost and sustainable strategy to prevent/attenuate obesity-related metabolic disorders, with potential applications in both food and pharmaceutical industries.

Conclusions

Our findings demonstrate that GPE protects against HFD-induced obesity, liver damage, inflammation and metabolic disturbances, in part by preserving intestinal barrier integrity and mitigating endotoxemia. These findings support the potential use of GP for counteracting obesity-related metabolic disorders, including NAFLD. More studies are needed to support the therapeutic potential of GPE in the prevention and/or treatment of metabolic alterations associated with obesity in humans.

Authors Contributions

M.A.V.P., P.I.O., E.C., and D.J.P. contributed to the conceptualization of the study, resources, and methodology. V.M.S. and D.J.P. conducted the investigation and formal analysis while V.M.S. and E.C. performed the *in vitro* investigation. V.M.S., D.J.P., E.C., and M.A.V.P performed data curation and formal analysis. V.V.C. was responsible for

animal handling procedures. A.R.F. conducted the chemical characterization of GPE. M.A.V.P., V.M.S., D.J.P., E.C., and P.I.O. drafted the original manuscript. M.A.V.P. was responsible for project administration. M.A.V.P. and P.I.O. were responsible for funding acquisition. All authors reviewed, edited, and approved the final version of the manuscript.

Conflict of Interest

The authors declare no conflicts of interest related to this work.

Data availability

The data supporting this article have been included as part of the Supplementary Information.

Acknowledgments

This work was supported by the Agencia Nacional de Promoción Científica y Tecnológica (Pict 2018-03056; Pict 2021-00397), PIP 0015-CONICET, National University of Cuyo [SIIP J037-T1] and Fundación Florencio Fiorini to M.V.P. Research in the P.I.O laboratory was funded by NIFA-USDA (grant CA-D-NTR-2819-H). P.I.O is an Honorary Researcher from CONICET, Argentina. V.M.S received a Fulbright fellowship. The graphical abstract was created using BioRender.com. We sincerely thank Dr. Julio Oliva for their valuable contribution in histological analysis, and Valeria Cacciamani for their outstanding technical assistance and dedication to animal handling throughout this study.

References

1. Phelps NH, Singleton RK, Zhou B, Heap RA, Mishra A, Bennett JE, et al. Worldwide trends in underweight and obesity from 1990 to 2022: a pooled analysis of 3663 population-representative studies with 222 million children, adolescents, and adults. The Lancet. 2024 Mar;403(10431):1027–50.

2. Blüher M. Obesity: global epidemiology and pathogenesis. Nat Rev Endocrinol. 2019 May 27;15(5):288–98.

3. Cani PD, Amar J, Iglesias MA, Poggi M, Knauf C, Bastelica D, et al. Metabolic Endotoxemia Initiates Obesity and Insulin Resistance. Diabetes. 2007 Jul 1;56(7):1761–72.

4. Carvalho BM, Abdalla Saad MJ. Influence of Gut Microbiota on Subclinical Inflammation and Insulin Resistance. Mediators Inflamm. 2013;2013:1–13.

5. Camilleri M. Leaky gut: mechanisms, measurement and clinical implications in humans. Gut. 2019 Aug;68(8):1516–26.

6. Bischoff SC, Barbara G, Buurman W, Ockhuizen T, Schulzke JD, Serino M, et al. Intestinal permeability – a new target for disease prevention and therapy. BMC Gastroenterol. 2014 Dec 18;14(1):189.

7. Suzuki T. Regulation of the intestinal barrier by nutrients: The role of tight junctions. Animal Science Journal. 2020 Jan 17;91(1).

8. Di Vincenzo F, Del Gaudio A, Petito V, Lopetuso LR, Scaldaferri F. Gut microbiota, intestinal permeability, and systemic inflammation: a narrative review. Intern Emerg Med. 2024 Mar 28;19(2):275–93.

9. Mouries J, Brescia P, Silvestri A, Spadoni I, Sorribas M, Wiest R, et al. Microbiota-driven gut vascular barrier disruption is a prerequisite for non-alcoholic steatohepatitis development. J Hepatol. 2019 Dec;71(6):1216–28.

10. Younossi ZM, Koenig AB, Abdelatif D, Fazel Y, Henry L, Wymer M. Global epidemiology of nonalcoholic fatty liver disease—Meta-analytic assessment of prevalence, incidence, and outcomes. Hepatology. 2016 Jul 22;64(1):73–84.

11. Seki E, Schnabl B. Role of innate immunity and the microbiota in liver fibrosis: crosstalk between the liver and gut. J Physiol. 2012 Feb 27;590(3):447–58.

12. Cremonini E, Iglesias DE, Matsukuma KE, Hester SN, Wood SM, Bartlett M, et al. Supplementation with cyanidin and delphinidin mitigates high fat diet-induced endotoxemia and associated liver inflammation in mice. Food Funct. 2022 Jan 24;13(2):781–94.

13. Iglesias DE, Cremonini E, Hester SN, Wood SM, Bartlett M, Fraga CG, et al. Cyanidin and delphinidin restore colon physiology in high fat diet-fed mice: Involvement of TLR-4 and redox-regulated signaling. Free Radic Biol Med. 2022 Aug;188:71–82.

14. Cremonini E, Daveri E, Mastaloudis A, Adamo AM, Mills D, Kalanetra K, et al. Anthocyanins protect the gastrointestinal tract from high fat diet-induced alterations in redox signaling, barrier integrity and dysbiosis. Redox Biol. 2019 Sep;26:101269.

15. Cremonini E, Wang Z, Bettaieb A, Adamo AM, Daveri E, Mills DA, et al. (-)-Epicatechin protects the intestinal barrier from high fat diet-induced permeabilization: Implications for steatosis and insulin resistance. Redox Biol. 2018 Apr;14:588–99.

16. Daveri E, Cremonini E, Mastaloudis A, Hester SN, Wood SM, Waterhouse AL, et al. Cyanidin and delphinidin modulate inflammation and altered redox signaling improving insulin resistance in high fat-fed mice. Redox Biol. 2018 Sep;18:16–24.

17. Vazquez Prieto MA, Bettaieb A, Rodriguez Lanzi C, Soto VC, Perdicaro DJ, Galmarini CR, et al. Catechin and quercetin attenuate adipose inflammation in fructose-fed rats and 3T3-L1 adipocytes. Mol Nutr Food Res. 2015 Apr 11;59(4):622–33.

18. Perdicaro DJ, Rodriguez Lanzi C, Gambarte Tudela J, Miatello RM, Oteiza PI, Vazquez

1. Phelps NH, Singleton RK, Zhou B, Heap RA, Mishra A, Bennett JE, et al. Worldwide trends in underweight and obesity from 1990 to 2022: a pooled analysis of 3663 population-representative studies with 222 million children, adolescents, and adults. The Lancet. 2024 Mar;403(10431):1027–50.

2. Blüher M. Obesity: global epidemiology and pathogenesis. Nat Rev Endocrinol. 2019 May 27;15(5):288–98.

3. Cani PD, Amar J, Iglesias MA, Poggi M, Knauf C, Bastelica D, et al. Metabolic Endotoxemia Initiates Obesity and Insulin Resistance. Diabetes. 2007 Jul 1;56(7):1761–72.

4. Carvalho BM, Abdalla Saad MJ. Influence of Gut Microbiota on Subclinical Inflammation and Insulin Resistance. Mediators Inflamm. 2013;2013:1–13.

5. Camilleri M. Leaky gut: mechanisms, measurement and clinical implications in humans. Gut. 2019 Aug;68(8):1516–26.

6. Bischoff SC, Barbara G, Buurman W, Ockhuizen T, Schulzke JD, Serino M, et al. Intestinal permeability – a new target for disease prevention and therapy. BMC Gastroenterol. 2014 Dec 18;14(1):189.

7. Suzuki T. Regulation of the intestinal barrier by nutrients: The role of tight junctions. Animal Science Journal. 2020 Jan 17;91(1).

8. Di Vincenzo F, Del Gaudio A, Petito V, Lopetuso LR, Scaldaferri F. Gut microbiota, intestinal permeability, and systemic inflammation: a narrative review. Intern Emerg Med. 2024 Mar 28;19(2):275–93.

9. Mouries J, Brescia P, Silvestri A, Spadoni I, Sorribas M, Wiest R, et al. Microbiota-driven gut vascular barrier disruption is a prerequisite for non-alcoholic steatohepatitis development. J Hepatol. 2019 Dec;71(6):1216–28.

10. Younossi ZM, Koenig AB, Abdelatif D, Fazel Y, Henry L, Wymer M. Global epidemiology of nonalcoholic fatty liver disease—Meta-analytic assessment of prevalence, incidence, and outcomes. Hepatology. 2016 Jul 22;64(1):73–84.

11. Seki E, Schnabl B. Role of innate immunity and the microbiota in liver fibrosis: crosstalk between the liver and gut. J Physiol. 2012 Feb 27;590(3):447–58.

12. Cremonini E, Iglesias DE, Matsukuma KE, Hester SN, Wood SM, Bartlett M, et al. Supplementation with cyanidin and delphinidin mitigates high fat diet-induced endotoxemia and associated liver inflammation in mice. Food Funct. 2022 Jan 24;13(2):781–94.

13. Iglesias DE, Cremonini E, Hester SN, Wood SM, Bartlett M, Fraga CG, et al. Cyanidin and delphinidin restore colon physiology in high fat diet-fed mice: Involvement of TLR-4 and redox-regulated signaling. Free Radic Biol Med. 2022 Aug;188:71–82.

14. Cremonini E, Daveri E, Mastaloudis A, Adamo AM, Mills D, Kalanetra K, et al. Anthocyanins protect the gastrointestinal tract from high fat diet-induced alterations in redox signaling, barrier integrity and dysbiosis. Redox Biol. 2019 Sep;26:101269.

15. Cremonini E, Wang Z, Bettaieb A, Adamo AM, Daveri E, Mills DA, et al. (-)-Epicatechin protects the intestinal barrier from high fat diet-induced permeabilization: Implications for steatosis and insulin resistance. Redox Biol. 2018 Apr;14:588–99.

16. Daveri E, Cremonini E, Mastaloudis A, Hester SN, Wood SM, Waterhouse AL, et al. Cyanidin and delphinidin modulate inflammation and altered redox signaling improving insulin resistance in high fat-fed mice. Redox Biol. 2018 Sep;18:16–24.

17. Vazquez Prieto MA, Bettaieb A, Rodriguez Lanzi C, Soto VC, Perdicaro DJ, Galmarini CR, et al. Catechin and quercetin attenuate adipose inflammation in fructose-fed rats and 3T3-L1 adipocytes. Mol Nutr Food Res. 2015 Apr 11;59(4):622–33.

18. Perdicaro DJ, Rodriguez Lanzi C, Gambarte Tudela J, Miatello RM, Oteiza PI, Vazquez Prieto MA. Quercetin attenuates adipose hypertrophy, in part through activation of adipogenesis in rats fed a high-fat diet. J Nutr Biochem. 2020 May;79:108352.

19. Negro C, Tommasi L, Miceli A. Phenolic compounds and antioxidant activity from red grape marc extracts. Bioresour Technol. 2003 Mar;87(1):41–4.

20. Liu W, Zhao S, Wang J, Shi J, Sun Y, Wang W, et al. Grape seed proanthocyanidin extract ameliorates inflammation and adiposity by modulating gut microbiota in high-fat diet mice. Mol Nutr Food Res. 2017 Sep;61(9):1601082.

21. Rodriguez Lanzi C, Perdicaro DJ, Antoniolli A, Fontana AR, Miatello RM, Bottini R, et al. Grape pomace and grape pomace extract improve insulin signaling in high-fat-fructose fed rat-induced metabolic syndrome. Food Funct. 2016;7(3):1544–53.

22. Rodriguez Lanzi C, Perdicaro DJ, Antoniolli A, Piccoli P, Vazquez Prieto MA, Fontana A. Phenolic metabolites in plasma and tissues of rats fed with a grape pomace extract as assessed by liquid chromatography-tandem mass spectrometry. Arch Biochem Biophys. 2018 Aug;651:28–33.

23. Machado TOX, Portugal I, Kodel H de AC, Droppa-Almeida D, Dos Santos Lima M, Fathi F, et al. Therapeutic potential of grape pomace extracts: A review of scientific evidence. Food Biosci. 2024 Aug;60:104210.

24. Antoniolli A, Fontana AR, Piccoli P, Bottini R. Characterization of polyphenols and evaluation of antioxidant capacity in grape pomace of the cv. Malbec. Food Chem. 2015 Jul;178:172–8.

25. Fontana A, Antoniolli A, D'Amario Fernández MA, Bottini R. Phenolics profiling of pomace extracts from different grape varieties cultivated in Argentina. RSC Adv. 2017;7(47):29446–57.

26. Rodriguez Lanzi C, Perdicaro DJ, Gambarte Tudela J, Muscia V, Fontana AR, Oteiza PI, et al. Grape pomace extract supplementation activates FNDC5/irisin in muscle and promotes white adipose browning in rats fed a high-fat diet. Food Funct. 2020;11(2):1537–46.

27. Perdicaro DJ, Rodriguez Lanzi C, Fontana AR, Antoniolli A, Piccoli P, Miatello RM, et al. Grape pomace reduced reperfusion arrhythmias in rats with a high-fat-fructose diet. Food Funct. 2017;8(10):3501–9.

28. Bettaieb A, Vazquez Prieto MA, Rodriguez Lanzi C, Miatello RM, Haj FG, Fraga CG, et al. (−)-Epicatechin mitigates high-fructose-associated insulin resistance by modulating redox signaling and endoplasmic reticulum stress. Free Radic Biol Med. 2014 Jul;72:247–56.

29. Kleiner DE, Brunt EM, Van Natta M, Behling C, Contos MJ, Cummings OW, et al. Design and validation of a histological scoring system for nonalcoholic fatty liver disease. Hepatology. 2005 Jun;41(6):1313–21.

30. Iglesias DE, Cremonini E, Oteiza PI, Fraga CG. Curcumin Mitigates TNFα-Induced Caco-2 Cell Monolayer Permeabilization Through Modulation of NF-κB, ERK1/2, and JNK Pathways. Mol Nutr Food Res. 2022 Nov 3;66(21).

31. Rao X, Huang X, Zhou Z, Lin X. An improvement of the 2ˆ(-delta delta CT) method for quantitative real-time polymerase chain reaction data analysis. Biostat Bioinforma Biomath. 2013 Aug;3(3):71–85.

32. Bradford MM. A rapid and sensitive method for the quantitation of microgram quantities of protein utilizing the principle of protein-dye binding. Anal Biochem. 1976 May;72(1–2):248–54.

33. Abenavoli L, Milic N, Di Renzo L, Preveden T, Medić-Stojanoska M, De Lorenzo A. Metabolic aspects of adult patients with nonalcoholic fatty liver disease. World J Gastroenterol. 2016;22(31):7006.

34. Vazquez-Prieto MA, Bettaieb A, Haj FG, Fraga CG, Oteiza PI. (−)-Epicatechin prevents TNFα-induced activation of signaling cascades involved in inflammation and insulin sensitivity in 3T3-L1 adipocytes. Arch Biochem Biophys. 2012 Nov;527(2):113–8.

35. Zhu W, Oteiza PI. Proanthocyanidins at the gastrointestinal tract: mechanisms involved in their capacity to mitigate obesity-associated metabolic disorders. Crit Rev Food Sci Nutr. 2024 Jan 13;64(2):220–40.

36. Porras D, Nistal E, Martínez-Flórez S, Pisonero-Vaquero S, Olcoz JL, Jover R, et al. Protective effect of quercetin on high-fat diet-induced non-alcoholic fatty liver disease in mice is mediated by modulating intestinal microbiota imbalance and related gut-liver axis activation. Free Radic Biol Med. 2017 Jan;102:188–202.

37. Martínez-Maqueda D, Zapatera B, Gallego-Narbón A, Vaquero MP, Saura-Calixto F, Pérez-Jiménez J. A 6-week supplementation with grape pomace to subjects at cardiometabolic risk ameliorates insulin sensitivity, without affecting other metabolic syndrome markers. Food Funct. 2018;9(11):6010–9.

38. Schirone L, Overi D, Carpino G, Carnevale R, De Falco E, Nocella C, et al. Oleuropein, a Component of Extra Virgin Olive Oil, Improves Liver Steatosis and Lobular Inflammation by Lipopolysaccharides–TLR4 Axis Downregulation. Int J Mol Sci. 2024 May 21;25(11):5580.

39. Bergheim I, Moreno-Navarrete JM. The relevance of intestinal barrier dysfunction, antimicrobial proteins and bacterial endotoxin in metabolic dysfunction-associated steatotic liver disease. Eur J Clin Invest. 2024 Jul 18;54(7).

40. NISHIKAWA S, YASOSHIMA A, DOI K, NAKAYAMA H, UETSUKA K. Involvement of Sex, Strain and Age Factors in High Fat Diet-Induced Obesity in C57BL/6J and BALB/cA Mice. Exp Anim. 2007;56(4):263–72.

41. Boursier J, Mueller O, Barret M, Machado M, Fizanne L, Araujo-Perez F, et al. The severity of nonalcoholic fatty liver disease is associated with gut dysbiosis and shift in the metabolic function of the gut microbiota. Hepatology. 2016 Mar 13;63(3):764–75.

42. Portincasa P, Bonfrate L, Khalil M, Angelis M De, Calabrese FM, D'Amato M, et al. Intestinal Barrier and Permeability in Health, Obesity and NAFLD. Biomedicines. 2021 Dec 31;10(1):83.

43. Biolato M, Manca F, Marrone G, Cefalo C, Racco S, Miggiano GA, et al. Intestinal permeability after Mediterranean diet and low-fat diet in non-alcoholic fatty liver disease. World J Gastroenterol. 2019 Jan 28;25(4):509–20.

44. Hu H, Lin A, Kong M, Yao X, Yin M, Xia H, et al. Intestinal microbiome and NAFLD: molecular insights and therapeutic perspectives. J Gastroenterol. 2020 Feb 16;55(2):142–58.

45. Damms-Machado A, Louis S, Schnitzer A, Volynets V, Rings A, Basrai M, et al. Gut permeability is related to body weight, fatty liver disease, and insulin resistance in obese individuals undergoing weight reduction. Am J Clin Nutr. 2017 Jan;105(1):127–35.

46. Carpino G, Del Ben M, Pastori D, Carnevale R, Baratta F, Overi D, et al. Increased Liver Localization of Lipopolysaccharides in Human and Experimental NAFLD. Hepatology. 2020 Aug 22;72(2):470–85.

47. Khanmohammadi S, Kuchay MS. Toll-like receptors and metabolic (dysfunction)-associated fatty liver disease. Pharmacol Res. 2022 Nov;185:106507.

48. Park BS, Lee JO. Recognition of lipopolysaccharide pattern by TLR4 complexes. Exp Mol Med. 2013 Dec 6;45(12):e66–e66.

49. Singh A, Koduru B, Carlisle C, Akhter H, Liu RM, Schroder K, et al. NADPH oxidase 4 modulates hepatic responses to lipopolysaccharide mediated by Toll-like receptor-4. Sci Rep. 2017 Oct 30;7(1):14346.

50. Zarkovic N. 4-Hydroxynonenal as a bioactive marker of pathophysiological processes. Mol Aspects Med. 2003 Aug;24(4–5):281–91.

51. Gil-Cardoso K, Ginés I, Pinent M, Ardévol A, Blay M, Terra X. The co-administration of proanthocyanidins and an obesogenic diet prevents the increase in intestinal permeability and metabolic endotoxemia derived to the diet. J Nutr Biochem. 2018 Dec;62:35–42.

52. Nishiumi S, Mukai R, Ichiyanagi T, Ashida H. Suppression of Lipopolysaccharide and Galactosamine-Induced Hepatic Inflammation by Red Grape Pomace. J Agric Food Chem. 2012 Sep 12;60(36):9315–20.

53. González-Mariscal L, Betanzos A, Nava P, Jaramillo BE. Tight junction proteins. Prog Biophys Mol Biol. 2003 Jan;81(1):1–44.

54. Kuo W, Odenwald MA, Turner JR, Zuo L. Tight junction proteins occludin and ZO-1 as regulators of epithelial proliferation and survival. Ann N Y Acad Sci. 2022 Aug 17;1514(1):21–33.

55. Al-Sadi R, Guo S, Ye D, Rawat M, Ma TY. TNF-α Modulation of Intestinal Tight Junction Permeability Is Mediated by NIK/IKK-α Axis Activation of the Canonical NF-κB Pathway. Am J Pathol. 2016 May;186(5):1151–65.

56. He WQ, Wang J, Sheng JY, Zha JM, Graham WV, Turner JR. Contributions of Myosin Light Chain Kinase to Regulation of Epithelial Paracellular Permeability and Mucosal Homeostasis. Int J Mol Sci. 2020 Feb 3;21(3):993.

57. Cremonini E, Mastaloudis A, Hester SN, Verstraeten S V., Anderson M, Wood SM, et al. Anthocyanins inhibit tumor necrosis alpha-induced loss of Caco-2 cell barrier integrity. Food Funct. 2017;8(8):2915–23.

58. Nunes C, Freitas V, Almeida L, Laranjinha J. Red wine extract preserves tight junctions in intestinal epithelial cells under inflammatory conditions: implications for intestinal inflammation. Food Funct. 2019;10(3):1364–74.

The data supporting this article have been included as part of the Supplementary Information.

Figure 1

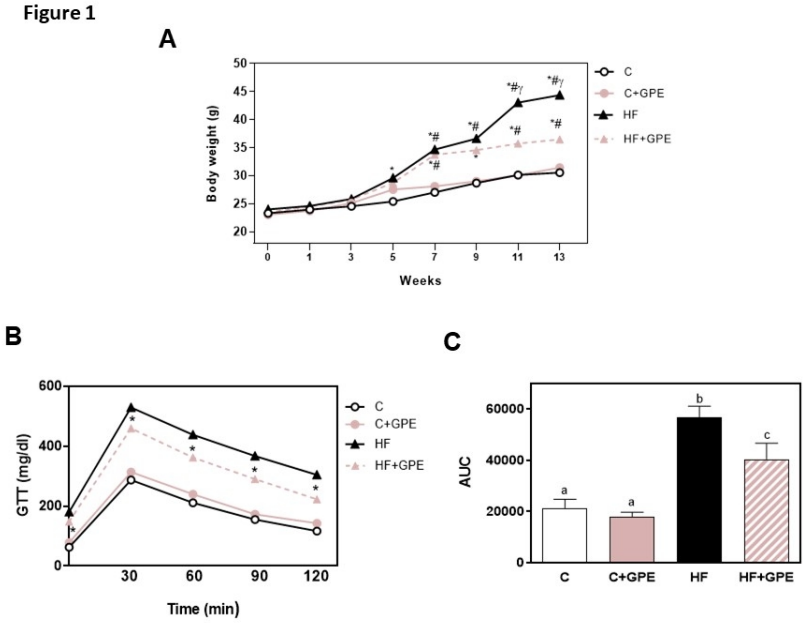

Figure 1. Effects of GPE supplementation on body weight and glucose tolerance test in mice fed control and high-fat diets. A. Body weight, B. Glucose Tolerance Test (GTT), and C. GTT Area Under the Curve (AUC). The GTT was done during week 10 of the dietary treatments. Mice were fed a control diet (empty circles, black bars) (C), a control diet supplemented with 300 mg of GPE (pink circles, pink bars) (C+GPE), a high-fat diet (black triangles, black bars) (HF), or a high-fat diet supplemented with 300 mg of GPE (pink triangles, pink striped bars) (HF+GPE) for 13 weeks. Results are shown as means ± SEM and are the average of 6-9 mice per group. Symbols used in graph A represent significant differences ($P<0.05$) as follow: * significantly different vs. C; # vs. C+GPE; γ vs. HF+GPE. C: Statistical significance ($P < 0.05$) is indicated by different superscripts (one-way ANOVA).

250x338mm (96 x 96 DPI)

Figure 2

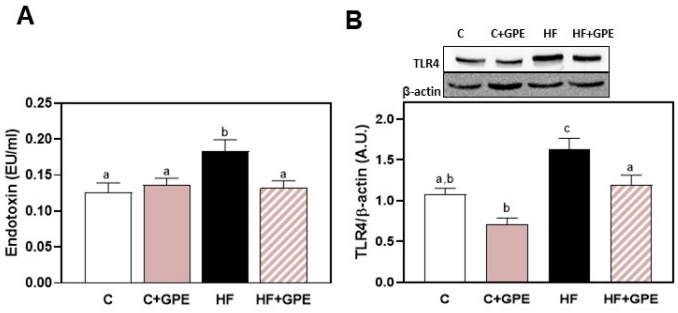

Figure 2. GPE supplementation attenuated HFD-induced endotoxemia and liver inflammation. Mice were fed either a control diet (C) or a HFD (HF) for 13 weeks, with or without 300 mg/kg body weight of GPE. At week 13, the following parameters were assessed: A. Plasma LPS concentration; B. TLR4 protein levels were assessed by Western blot. Bands were quantified, and values were normalized to β-actin levels. Results are shown as means ± SEM, representing the average of 6-9 mice per group. Statistical significance ($P < 0.05$) is indicated by different superscripts (one-way ANOVA).

250x338mm (96 x 96 DPI)

Figure 3

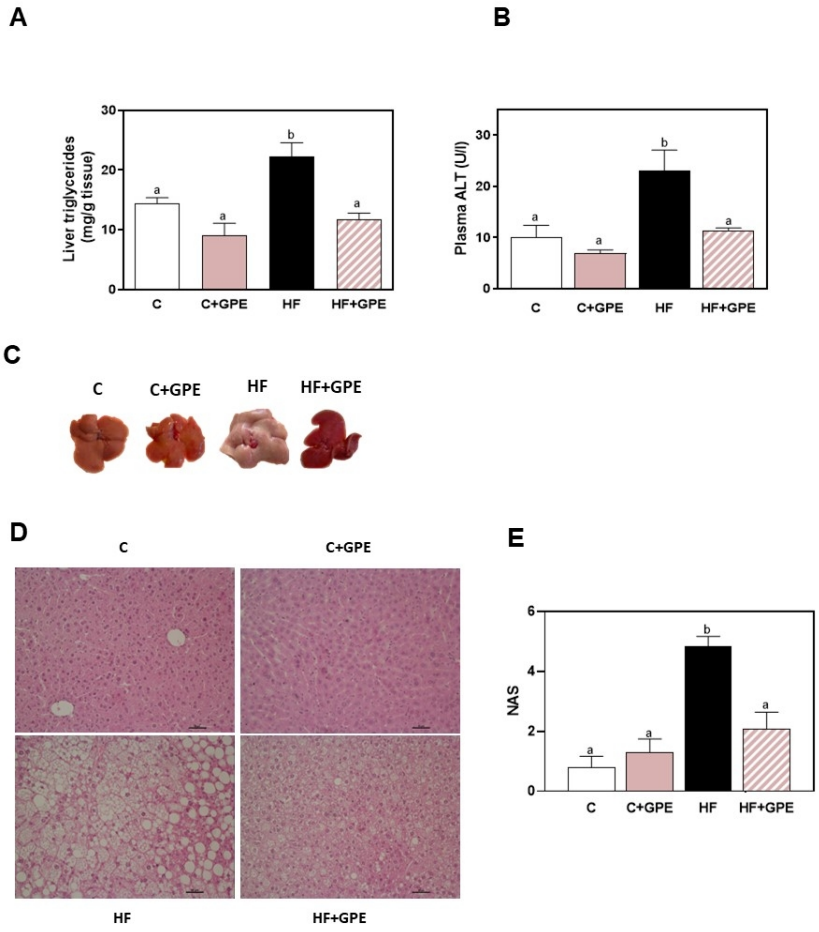

Figure 3. Effect of GPE on parameters of liver damage and steatosis. Mice were fed either a control diet (C) or a HFD (HF) for 13 weeks, with or without 300 mg/kg body weight of GPE. At week 13, the following parameters were assessed: A. Liver triglyceride content (mg/g); B. Plasma alanine aminotransferase (ALT) activity (U/L); C. Liver images; D. Representative liver sections stained with Hematoxylin & Eosin (H&E) Images are shown at 20x magnification; and E. NAFLD activity score (NAS), evaluated as described in methods. All results are shown as means ± SEM of 6-9 mice per group. Statistical significance ($P < 0.05$) is indicated by different superscripts (one-way ANOVA).

250x338mm (96 x 96 DPI)

Figure 4

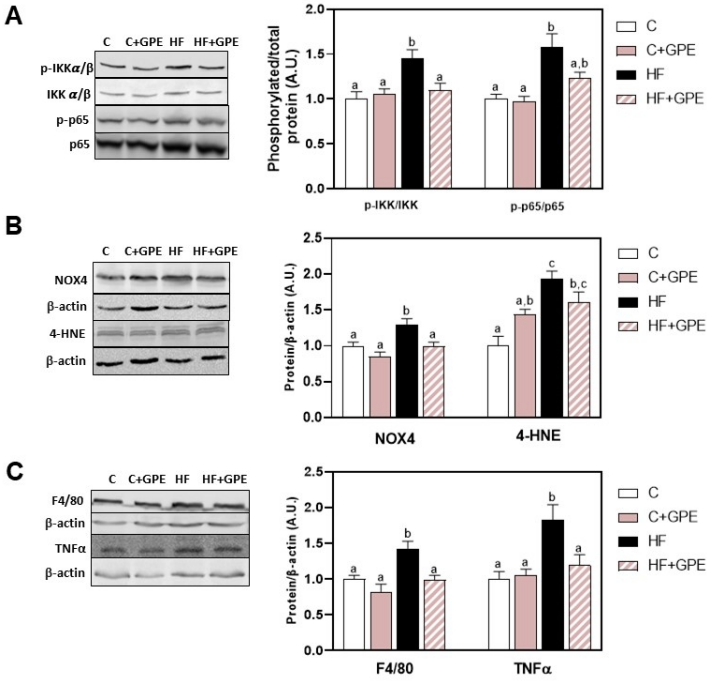

Figure 4. Effect of GPE on NF-κB activation and downstream expression of inflammatory protein in the liver. Mice were fed either a control diet (C) or a HFD (HF) for 13 weeks, with or without 300 mg/kg body weight of GPE. At week 13, the following parameters were assessed in the liver: A. Phosphorylation of IKK (Ser178/180) and p65 (Ser536); and protein levels of B. NOX4 and 4-HNE; and C. F4/80 and TNFα were measured by Western blot. Band intensities were quantified, with values normalized to total protein levels (for p65 and IKK) or to β-actin (used as a loading control for NOX4, F4/80, and TNFα). All results for C+GPE, HF, and HF+GPE groups were referred to the C group values. Results are shown as mean ± SEM of 6–9 mice per group. Statistical significance ($P < 0.05$) is indicated by different superscripts (one-way ANOVA).

250x338mm (96 x 96 DPI)

Figure 5

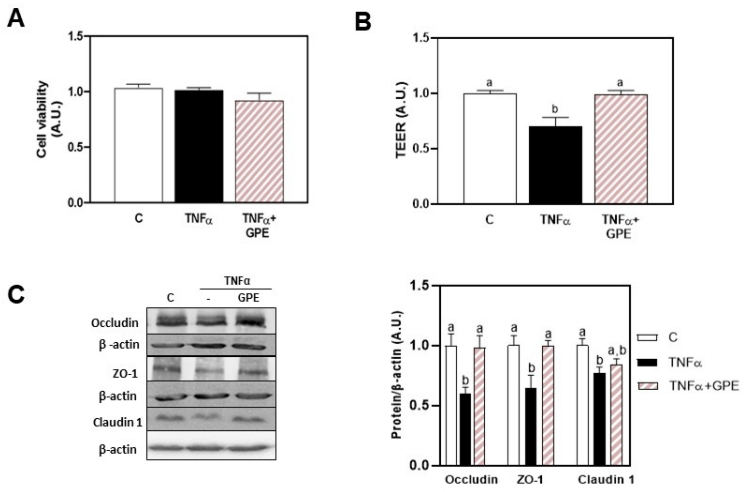

Figure 5. Effects of GPE on Caco-2 cell monolayer permeabilization induced by TNFα and TJ protein levels. A. Cell viability was evaluated using the MTT method in cells incubated without or with GPE (25 µg/ml) for 30 minutes and then in the absence or the presence TNFα (10 ng/ml) for further 6 h; B. Transepithelial Electrical Resistance (TEER) was measured in Caco-2 Cells cultured in transwell inserts: Polarized cells were incubated for 6 hours at 37°C under three conditions: 1. Control (C, no additions), 2. TNFα (10 ng/mL) added to the lower chamber, and 3.TNFα (10 ng/mL) added to the lower chamber and GPE (25 µg/ml) added to the upper chamber 30 min prior TNFα addition. Results are shown as mean ± SEM of 5 independent experiments. C. Protein levels of occludin, ZO-1, and claudin-1 were measured by Western blot after 6 h in the corresponding treatments and values referred to β-actin levels. Results are shown as mean ± SEM of 3–5 independent experiments. Data were normalized to control values. Statistical significance ($P < 0.05$) is indicated by different superscripts (one-way ANOVA).

250x338mm (96 x 96 DPI)

Figure 6

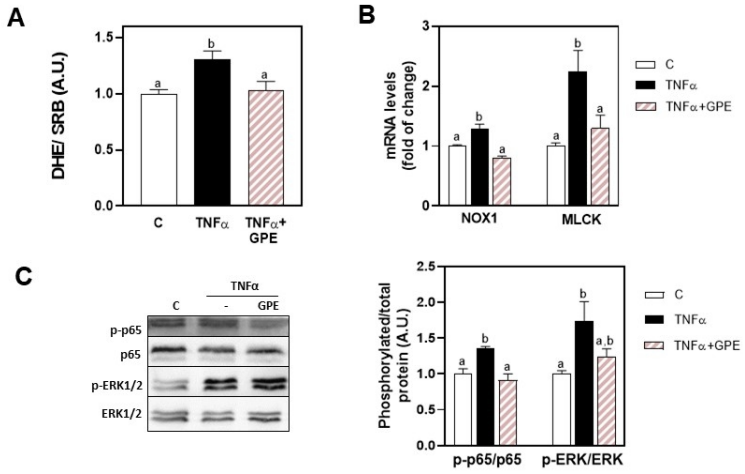

Figure 6. Effects of GPE on TNFα-induced oxidative stress in Caco-2 cells. Cells were incubated without or with GPE (25 µg/ml) for 30 minutes and then in the absence or the presence TNFα (10 ng/ml) for further 10 minutes A. Oxidation of the fluorescent probe DHE was assessed as described in methods and DHE (oxidized DHE) fluorescence was normalized to sulforhodamine B (SRB) absorbance. B. NOX1 and MLCK mRNA levels were determined by qPCR after 6 h and 3 h of incubation with TNFα, respectively, and the relative gene expression was normalized to β-actin as a housekeeping gene. Results are shown as mean ± SEM of four to five independent experiments, with data normalized to control values; and C. After 5 minutes of incubation with TNFα, phosphorylation of p65 (Ser536) and after 30 minutes of incubation, phosphorylation of ERK1/2 (Thr202/Tyr204), were measured by Western blot. Bands were quantified, and values were normalized to total protein levels (p65, ERK1/2). Results are shown as mean ± SEM of 3-5 independent experiments. Statistical significance ($P < 0.05$) is indicated by different superscripts (one-way ANOVA).

250x338mm (96 x 96 DPI)

Analyte	Concentration ($\mu g\ g^{-1}$ GPE)
Hydroxybenzoic acids	
Gallic acid	342.4 ± 19.7
Syringic acid	322.0 ± 16.7
Total	**664.3**
Hydroxycinnamic acids	
Caftaric acid n.d.	342.4 ± 19.7
p-coumaric acid	24.4 ± 1.7
Ferulic acid	22.9± 1.4
Total	**389.7**
Stilbene	
Polydatin	4234.1 ± 293.4
trans-resveratrol	51.6 ± 2.1
E-viniferin	19.5 ± 4.1
Total	**4395.2**
Flavanols	
(+)-catechin	5768.0 ± 333.0
(−)-epicatechin	3745.6 ± 194.6
Procyanidin B1	268.5 ± 17.0
Procyanidin B2	579.8 ± 38.5
Total	**10361.9**
Flavonols	
Quercetin 557±48	1269.8 ± 73.3
Fisetin	1041.8 ± 54.2
Isorhamnetin	10.0 ± 0.6
Total	**2321.6**
Other compounds	
OH-tyrosol	76.7 ± 4.0
Tyrosol	23.7 ± 1.1
Genistin	12.4 ± 0.6
Total	**112.8**
Total LMW-PPs	**18245.5**
TPC	**194.6 ± 0.7***

Table 1. Concentrations of LMW-PPs and total phenolic content (TPC) in freeze-dried Malbec GPE: TPC: *mg of GAE per g GPE. Values are shown as means ± SEM, n=3 replicates.

Analyte	Concentration ($\mu g\ g^{-1}$ GPE)
Anthocyanins glucosides	
Delphinidin 3-O-Glucoside	1900 ± 76.8
Cyanidin 3-O-Glucoside	284 ± 13.3
Petunidin 3-O-Glucoside	2396 ± 124.7
Peonidin 3-O-Glucoside	818 ± 269.0
Malvidin 3-O-Glucoside	9066 ± 471.1
Total	**14464**
Anthocyanins acetyl glucosides	
Delphinidin 3-O acetylglucoside	344 ± 13.9
Petunidin 3-O acetylglucoside	309 ± 14.4
Peonidin 3-O acetylglucoside	354 ± 13.9
Malvidin 3-O acetylglucoside	1520 ± 64.1
Total	**2527**
Anthocyanins coumaroyl glucosides	
Cyanidin 3-p-coumaroylglucoside	274 ± 14.4
Petunidin 3-p-coumaroylglucoside	484 ± 16.2
Peonidin 3-p-coumaroylglucoside	1070 ± 42.7
Malvidin 3-p-coumaroylglucoside	14152 ± 792.7
Total	**15980**
Total anthocyanins	**32971**

Table 2. Concentrations of individual anthocyanins in freeze-dried Malbec GPE: The concentrations of individual anthocyanin in the GPE were categorized by the type of derivative (non-acylated, acylated, and coumarylated). Values are shown as means ± SEM, n=3 replicates.

Table 3. Physiological Outcomes and Metabolic Measures

	C	C+GPE	HF	HF+GPE
Food intake (g/day)	3.0 ± 0.1	2.9 ± 0.2	2.6 ± 0.1	2.6 ± 0.1
Caloric intake (Kcal/g/day)	10.8 ± 0.3 [a]	10.4 ± 0.6 [a]	13.1 ± 0.6 [b]	13.2 ± 0.5 [b]
Final Body weight (g)	30.6 ± 1.4 [a]	29.9 ± 1.6 [a]	44.1 ± 0.7 [b]	36.44 ± 1.2 [c]
vWAT/BW (g/g)	3.8 ± 0.5 [a]	4.9 ± 0.8 [a]	9.6 ± 0.4 [b]	7.3 ± 0.3 [c]
sWAT/BW (g/g)	4.2 ± 0.6 [a]	5.5 ± 0.8 [a]	11.4 ± 0.5 [b]	7.9 ± 0.3 [c]
Liver/BW (g/g)	4.0 ± 0.1 [a]	4.1 ± 0.1 [a]	3.9 ± 0.3 [a]	3.1 ± 0.1 b
Fasted glucose (mg/dl)	62.5 ± 4.9 [a]	78.0 ± 2.1 [a]	177.0 ± 7.8 [b]	142.2 ± 9.7 [c]
Fasted Insulin (ng/ml)	0.1 ± 0.0 [a]	0.2 ± 0.1 [a,b]	0.8 ± 0.1 [c]	0.3 ± 0.0 [b]
HOMA:IR	0.5 ± 0.1 [a]	0.5 ± 0.1 [a]	10.0 ± 0.8 b	3.9 ± 0.8 [c]
Total cholesterol (mg/dl)	84.7 ± 6.2 [a]	92.0 ± 6.3 [a]	140.2 ± 14.3 [b]	115.1 ± 4.0 [a,b]
LDL cholesterol (mg/dl)	81.9 ± 6.1 [a]	84.1 ± 5.2 [a]	125.1 ± 10.0 [b]	94.7 ± 11.9 [a,b]
Triglycerides (mg/dl)	36.4 ± 4.1 [a,b]	37.1 ± 3.8 [a,b]	50.1 ± 4.5 [a]	27.3 ± 4.3 [b]

Table 3. Effects of supplementation of GPE on food and caloric intake and metabolic parameters: Mice were provided a control diet (C) or a high-fat diet (HF) for 13 weeks, with or without 300 mg/kg body weight of GPE. Food intake was assessed every 7 days throughout the experimental protocol. The ratio of visceral and subcutaneous adipose tissue and liver weight to body weight were also recorded. Plasma levels of glucose, insulin, total cholesterol, LDL cholesterol, and triglycerides were measured. Values are shown as means ± SEM (8-9 animals per group). Statistical differences between groups are indicated by distinct superscripts ($P < 0.05$, one-way ANOVA).